Cold exposure drives weight gain and adiposity following chronic suppression of brown adipose tissue

Peter Aldiss[1*], Jo E Lewis[3], Irene Lupini[4], Ian Bloor[1], Ramyar Chavoshinejad[1], David Boocock[5], Amanda K Miles[5], Francis J P Ebling[3], Helen Budge[1] and Michael E Symonds[1, 2*].

[1] *The Early Life Research Unit, Division of Child Health, Obstetrics and Gynaecology, School of Medicine, University of Nottingham;* peter.aldiss@nottingham.ac.uk*; helen.budge@nottingham.ac.uk; michael.symonds@nottingham.ac.uk; ian.bloor@nottingham.ac.uk; ramyar.chavoshinejad@nottingham.ac.uk*

[2] *Nottingham Digestive Disease Centre and Biomedical Research Unit, School of Medicine, University of Nottingham*

[3] *School of Life Sciences, Queen's Medical Centre, University of Nottingham; fran.ebling@nottingham.ac.uk; jl2033@medschl.cam.ac.uk*

[4] *School of Biosciences and Veterinary Medicine, University of Camerino, Camerino, MC, Italy; Irene.lupini@studenti.unicam.it*

[5] *John van Geest Cancer Research Centre, Nottingham Trent University, Nottingham, NG11 8N; david.boocock@ntu.ac.uk; amanda.miles@ntu.ac.uk*

***** Correspondence: peter.aldiss@nottingham.ac.uk; *michael.symonds@nottingham.ac.uk*

Declaration of interests: None

Abstract

Therapeutic activation of thermogenic brown adipose tissue (BAT) may be feasible to prevent, or treat, cardiometabolic disease. However, rodents are commonly housed below thermoneutrality (~20°C) which can modulate their metabolism and physiology including the hyperactivation of brown (BAT) and beige white adipose tissue. We housed animals at thermoneutrality from weaning to chronically supress BAT, mimic human physiology and explore the efficacy of chronic, mild cold-exposure and β3-adrenoreceptor agonism under these conditions. Using metabolic phenotyping and exploratory proteomics we show that transfer from 28°C to 20°C drives weight gain and a 125% increase in subcutaneous fat mass, an effect not seen with YM-178 administration thus suggesting a direct effect of a cool ambient temperature in promoting weight gain and further adiposity in obese rats. Following chronic suppression of BAT, uncoupling protein 1 mRNA was undetectable in IWAT in all groups. Using exploratory adipose tissue proteomics, we reveal novel gene ontology terms associated with cold-induced weight gain in BAT and IWAT whilst Reactome pathway analysis highlights the regulation of mitotic (i.e. G2/M transition) and metabolism of amino acids and derivatives pathways. Conversely, YM-178 had minimal metabolic-related effects but modified pathways involved in proteolysis (i.e. eukaryotic translation initiation) and RNA surveillance across both tissues. Taken together these findings are indicative of a novel mechanism whereby animals increase body weight and fat mass following chronic suppression of adaptive thermogenesis from weaning. In addition, treatment with a B3-adrenoreceptor agonist did not improve metabolic health in obese animals raised at thermoneutrality.

Keywords: brown adipose tissue, thermoneutrality, healthy expansion of adipose tissue, proteomics

Introduction

Therapeutic activation of thermogenic brown adipose tissue (BAT) may be feasible to prevent, or treat, cardiometabolic disease [1]. In rodent models of obesity, the activation of BAT and uncoupling protein (UCP1)-positive beige adipocytes in white adipose tissue (WAT) by cold exposure and sympathomimetics (i.e. β3-agonists) can attenuate or reverse obesity, diabetes and atherosclerosis, thus improving metabolic health [1]. A major factor influencing these outcomes is that animals are typically housed at temperatures well below their thermoneutral zone (which for a rodent is c. 28°C) [2]. Under these conditions, not only is BAT hyperactive, but UCP1+ beige adipocytes are readily seen in the inguinal WAT (IWAT) depot [3].

The 'cold-stressed' animal has been widely studied but much less is known about the underlying adaptations in adipose tissue of animals maintained at thermoneutrality. Usually, temperatures as low as 4°C, which represent an 'extreme cold', are used to activate BAT, with the induction of UCP1 and subsequent thermogenic response primarily seen in subcutaneous IWAT and other 'beige' depots [3]. Conversely, when animals are housed at thermoneutrality and then exposed to 20°C, the induction of UCP1 is primarily seen in BAT. These differences suggest there are two steps to the 'browning' process and emphasise the need to study rodent metabolism under thermoneutral conditions. Importantly, it was recently demonstrated that BAT from obese mice, housed chronically at thermoneutrality closely resembles human BAT [4]. This model of 'physiologically humanised BAT' is now thought to represent the best choice for studying the physiology of this key metabolic tissue [4]. Here, we extend this recent work by raising animals at thermoneutrality, on an obesogenic diet from weaning. Beginning this early is a particularly important consideration given the early developmental steps which would be occurring in early life [5]. Furthermore, we use rats as classically, their physiology to external stressors such as diet and the environment is closer, than mice, to humans [6]. Using this model we have demonstrated UCP1 mRNA is absent in subcutaneous IWAT (the classical 'beige' depot) and not induced with exercise training [7], a common response at standard housing temperatures and one which is typically not seen in humans [8]. We hypothesised that activation of BAT by mild-cold and YM-178, a highly selective β3-agonist that was recently been shown to activate BAT in lean and obese humans, and drive improvements in lipid metabolism, would be negligible under these conditions [9, 10]. Moreover, perivascular BAT would be more responsive as previously shown to be the case with exercise training [7]. Finally, we sought to determine how the AT proteome responds following chronic BAT suppression to better understand the molecular response to potentially thermogenic stimuli at thermoneutrality.

Results

Four weeks of exposure to 20°C promoted weight gain and increased BAT and subcutaneous IWAT mass, an effect not seen with a clinically relevant dose of YM-178 (Fig. 1A-E). There was no change in total fat mass (i.e. the total of all dissected depots), gonadal (GWAT), mesenteric (MWAT), retroperitoneal (RPWAT) or paracardial (PCAT) fat depots, or in liver or heart mass (Fig. 1C and Supp. Fig 1B-G) suggesting cold does not drive whole body changes in adiposity, and potentially lean mass. There was however a significant increase in kidney size (Supp. Fig 1H). As there was no difference in 24h energy expenditure, or intake, (Supp. Fig. 1I-J) we incorporated these parameters, alongside body mass, into an ANCOVA. Whilst there was no evidence that changes in body mass were associated with altered energy expenditure (Fig. 1G) in cold exposed rats there was a significant, unexpected relationship between body mass and energy intake in this group (r^2=0.852, p=0.025, Fig. 1H) which was not seen in animals treated with YM-178. (Fig. 1A-H). Increased weight gain and adiposity in cold-exposed animals was not associated with impaired metabolic parameters (i.e. serum glucose, triglycerides and NEFA) or hormones (i.e. insulin and leptin) (Fig. 1I-N) suggesting it is not pathological.

Neither cold exposure, nor YM-178 were effective at inducing thermogenic genes (i.e. UCP1) in BAT or PVAT. in (Fig. 1O-P). Expression of the BAT marker CITED1 and beige marker TMEM26 were reduced in BAT of both cold exposed and YM-178 treated rats whilst the beige marker P2RX5 was upregulated in PVAT. Using targeted arrays to screen for primary genes involved in adipose tissue metabolism we saw an increase in the expression of FASN mRNA in both BAT and PVAT (Fig.1O-P). There was also an increase of genes involved in glycolysis (i.e. HK2 and PDK), fatty acid oxidation (i.e. ACACA and ACACB) and insulin resistance (i.e. AdipoR1 and MAPK9) in PVAT only following cold exposure (Fig. 1R-W). In contrast, in IWAT, UCP1 mRNA (Fig. 1Q).was absent in all rats and, despite a c.125% increase in IWAT mass of cold exposed rats, there was no change in the expression of other genes associated with thermogenesis (i.e. ADRβ3), beige adipocytes (i.e. TMEM26) or lipogenesis (i.e. FASN).

Morphologically, BAT was characterised by a heterogenous mix of small, mitochondria rich lipid droplets and large lipid droplets, and adipocytes, indicative of large-scale whitening (Fig. 2A). Analysis of lipid droplet area in BAT demonstrated a significant increase in both cold, and YM-178 treated rats (Fig. 2B). Adipocyte size also increased in IWAT of cold-exposed rats (Fig. 3A and B). Given the surprising increase in BAT and IWAT mass with cold exposure, we then carried out exploratory adipose tissue proteomics. This method, which quantifies the 30-40% most abundant proteins across samples, did not detect UCP1 in BAT

which is not unexpected given the chronic suppression of adaptive thermogenesis. We identified 175 differentially regulated proteins in BAT of cold-exposed rats (Fig. 2C, Table 1 and supp. data) including an increase in the mitochondrial citrate transporter protein (SLC25a1), glucose-6-phosphate dehydrogenase (G6PD), and the muscle isoforms of phosphoglycerate mutase (PGAM2) and creatine kinase (CKm).

Conversely, 137 proteins were differentially regulated in BAT of YM-178 treated animals (Fig. 2C, Table 1 and supp. data) with an upregulation of proteins involved in skeletal muscle physiology including myosin heavy chain 4 (MYH4), the fast-twitch skeletal muscle isoforms troponin I2 (TNNI2) and calsequestrin 1 (CASQ1in addition to proteins governing endothelial adhesion and vascular growth (PECAM1 and FBLN5). These changes occurred alongside a downregulation of the aldo-keto reductase family member proteins B15 (AKR1B15) and C3 (AKR1C3), mevalonate diphosphate decarboxylase (MVD), trans-2,3-enoyl-CoA reductase (TECR), acyl-CoA dehydrogenase short/branched chain (ACADSB), phosphate cytidylyltransferase 1, choline, alpha (PCYT1A) and 3-hydroxybutyrate dehydrogenase 1 (BDH1) proteins.

We then carried out functional analysis of the BAT proteome. The differentially regulated proteins in BAT of cold exposed animals enriched GO terms involved '*glucose import*', '*ATP-dependent helicase activity'* and '*regulation of protein phosphorylation'* whilst there was also an enrichment of nuclear related GO terms including '*histone deacetylation'*, '*nucleosomal DNA binding'*, '*nuclear chromatin'* and the '*nucleosome'* (Table 2 and supp. data). Conversely, differentially regulated proteins in BAT of animals treated with YM-178 enriched GO terms including '*positive regulation of protein kinase B signalling'*, '*negative regulation of cellular carbohydrate metabolic process'* and '*positive regulation of atpase activity'* whilst there was also an enrichment of GO terms involved in both brown adipocyte and muscle biology including '*brown fat cell differentiation'*, '*skeletal muscle contraction'* and '*regulation of muscle contraction'* (Table 2 and supp. data). Finally, using ReactomePA we show enriched pathways regulated by cold exposure (Fig. 2D), and their interactions (Fig. 2E), including 'transcriptional regulation of RUNx1', pathways involved in mitosis (i.e. G2/M transition), and the degradation of glycoproteins (i.e. CS/DS degradation). Conversely, YM-178 treatment enriched multiple pathways associated with proteolysis (i.e. eukaryotic translation initiation and formation of a pool of free 40S subunits) and RNA surveillance (i.e. nonsense mediated decay) (Fig. 2F and G).

The substantial increase in IWAT of cold-exposed rats was associated with 116 differentially regulated proteins (Fig. 3C, Table 3 and supp. data) including the upregulation of lipid metabolic proteins such as fatty acid binding proteins 1 (FABP1) and 3 (FABP3), fatty acid

synthase (FASN) and ATP citrate lyase (ACLY) and those involved in beta oxidation including hydroxynacyl-CoA dehydrogenase (HADH) and acyl-CoA dehydrogenase long chain (ACADL). In addition, there was an upregulation of glycerol kinase (GK), pyruvate carboxylase (PC) and monocarboxylic acid transporter 1 (MCT1) that were accompanied by a downregulation of multiple proteins involved in mRNA processing and splicing (i.e. RNA binding motif protein 8B, RBM8B; dexd-Box helicase 39B, DDX39B and poly(u) binding splicing factor 60, PUF60).

YM-178 administration modulated 206 proteins in IWAT (Fig. 3C, Table 3 and supp. data) including an upregulation of multiple proteins involved in the nervous system including synuclein gamma (SNCG), neurolysin (NLN) and neuronal pas domain protein 4 (NPAS4). This was associated with an increase in proteins involved in lipid and cholesterol metabolism including carnitine palmitoyltransferase 1A (CPT1A), hormone-sensitive lipase (LIPE) and apolipoprotein C1 and M (APOC1 and APOM). Interestingly, YM-178 also induced an increase in multiple inflammatory proteins, including orosomucoid 1 (ORM1), complement C4A (C4A), S100 calcium binding protein A8 (S100A8) and S100 calcium binding protein B (S100B).

Differentially regulated proteins in IWAT of cold-exposed rats enriched GO terms involved in the '*DNA damage response', '3-hydroxyacyl-coa dehydrogenase activity'* and '*NAD+ binding'* whilst YM-178 enriched inflammatory terms including the *'acute phase response'* and *'structural constituent of ribosome'* suggesting an effect of sympathetic activation on both the inflammatory system and protein synthesis (Table 4 and supp. data). Finally, ReactomePA demonstrated enriched pathways (Fig. 3D), and their interactions (Fig. 3E) were associated with IWAT expansion including the 'metabolism of amino acids and derivatives' and 'fatty acid metabolism'. Conversely, and similar to BAT, YM-178 treatment enriched multiple pathways associated with proteolysis (i.e. eukaryotic translation initiation and formation of a pool of free 40S subunits) and RNA surveillance (i.e. nonsense mediated decay) but to a larger degree (i.e. 23-27 proteins per term rather than 9-11; Fig. 3F and G).

Discussion

Housing temperature, especially cold exposure, impacts on metabolic homeostasis as illustrated by the effects on BAT and 'browning' [3, 11-14]. Little is known as to whether interventions considered to promote browning are effective in animals maintained at thermoneutrality [2, 14]. Here we show that chronic exposure to a mild-cold stimulus (i.e. standard housing temperature) drives weight gain and the deposition of large quantities of

subcutaneous adipose tissue in obese rats rather than the activation of BAT and subsequent weight-loss as expected [1]. This effect is not seen in rats treated with the highly selective β3-agonist YM-178, suggesting sympathetic activation is not involved and a direct effect of ambient temperature. Taken together these findings are indicative of a novel mechanism whereby rats increase body weight and fat mass following chronic suppression of adaptive thermogenesis from weaning.

There is accumulating evidence that, in the absence of adaptive thermogenesis, other mechanisms compensate in order to maintain body temperature. For instance, in UCP1 k/o mice, a reduction in BAT thermogenesis leads to a the recruitment of shivering thermogenesis in skeletal muscle [15]. Conversely, when shivering is impaired in Sarcolipin k/o mice, there is a compensatory increase in BAT activity [15]. In obese animals lacking BAT, there seems to be an entirely different homeostatic response to cold stress. Following BAT lipectomy, obese, cold-exposed rats gain weight and adipose tissue mass is nearly doubled [16] which mirrors our findings when BAT is chronically supressed. Furthermore, intermittent cold-exposure (from 20°C to 4°C) over a period of days promotes weight gain and adiposity and this is associated with intermittent increases in energy intake [17]. Rats are also more susceptible to weight gain, and fat accumulation when reared in the cold (18°C vs. 30°C), an effect which persists when housed at a common temperature [18]. There is also a plausible mechanism linking the gut to this phenotype which needs to be explored. Cold exposure drives intestinal growth, increased fatty acid absorption and paracellular permeability to nutrients [19, 20]. The efficiency of energy utilisation is also sufficient to maintain core body temperature during acute cold exposure [21]. If the gut can grow, even during periods of energy restriction, and maximise absorption of energy to a degree that it sustains critical functions, and ultimately life, then it may be able to drive adiposity in a similar manner. Whilst the insulative effects of obesity are being debated [22-24] a model whereby rats, and potentially other rodents, deposit subcutaneous fat during exposure to cold (i.e. “store up nuts for the winter internally” [18]) would make sense, and be hugely beneficial from an evolutionary perspective given wild animals cannot simply increase energy intake during winter months.

Another important finding of this study is that the increase in weight gain and subcutaneous AT mass seen in cold-exposed rats was not associated with impaired metabolic parameters (i.e. fasting glucose and lipids) or any discernible adipose tissue dysfunction. Here, chronic exposure to a mild cold stimulus seemingly drives a phenotypically healthy expansion of subcutaneous AT. Using exploratory proteomics, we were able to elucidate processes in

both BAT and IWAT associated with this expansion of AT mass. An increase in proteins that modulate metabolism, including those involved in glycolysis, the TCA cycle and lipogenesis, suggests that there is an increased metabolic flux in these depots which, ultimately, results in net lipogenesis. In BAT, this is associated with an enrichment of mitotic pathways (i.e. G2/M transition). The G2/M transition is a critical point in the cell cycle where, following DNA replication, the mitotic process begins, and cells separate into replicate daughter cells. Mitotic clonal expansion is essential for adipogenesis in 3T3-L1 adipocytes [25] and is one of the postulated mechanisms through which FTO regulates fat mass [26]. Further, enrichment of the 'transcriptional regulation on RUNX1' pathway, which regulates the white-to-brown/beige transition via CDK6 points towards the cell-cycle as a key mediator of increased BAT mass following cold-exposure [27]. As such, an increase in mitosis of adipocyte pre-cursors, key changes in the cell cycle and subsequent adipogenesis may be partly driving increased BAT mass.

In IWAT, an upregulation of regulatory proteins involved in lipid metabolism (i.e. FABP1, FASN and ACLY) and beta oxidation (i.e. HADH and ACADL) in addition to GK, PC and MCT1 indicates an increased metabolic flux in IWAT. Importantly, however, adipocyte size in IWAT of cold-exposed rats only increased by ~17%. As such, we predict that this physiological expansion of IWAT is largely due to adipogenesis which ties in to the already established theorem of 'healthy adipose tissue expansion' where growth of subcutaneous AT, through adipogenesis, protects from the adverse effects of an obesogenic diet [28].

We were also able to elucidate the impact of sympathetic activation in the absence of any change in housing temperature by administering YM-178. This highly selective β3-agonist increases BAT activity, whole body EE and induces 'browning' in humans [29-32]. More recently, two landmark studies have demonstrated that YM-178 also improves glucose homeostasis and insulin sensitivity, improves β-cell function, reduces skeletal muscle triglyceride content and increases HDL cholesterol and adiponectin in overweight and obese prediabetic or insulin resistant humans [9, 10]. However, these, and other studies show that human BAT activity and the response to either cold, or other thermogenic stimuli (i.e. YM-178) is highly heterogenous which is unsurprising given humans undergo seasonal BAT activation to varying degrees [33]. Our aim was to determine the efficacy of this treatment in a homogenous population where BAT had been supressed from early life. Under these conditions, YM-178 treatment had no impact on metabolic parameters or thermogenesis. It does, however, effect pathways involved in protein synthesis in both BAT and, to a larger degree, IWAT. In the hippocampus, β3-AR agonism (by isoprenaline) drives ERK/MTOR dependent activation of eukaryotic initiation factor 4E and inhibition of the translation repressor 4E-BP whilst CL316, 243 and salbutamol drive skeletal muscle hypertrophy and

protein synthesis in mice and humans respectively [34-36]. This would suggest a novel role for YM-178 in regulating protein synthesis in adipose tissues which has yet to be examined with previous human studies focussing on overactive bladder and associated symptoms [36, 37]. YM-178 also impacted on proteins involved in the acute phase response and inflammation in both BAT and IWAT. Taken together, this suggests that YM-178 treatment following chronic suppression of BAT may act negatively on AT driving inflammatory processes. Whilst these differences may be species specific, they may also highlight potential effects of YM-178 if given to individuals lacking BAT, or who exhibit low responsiveness to thermogenic stimuli.

Whilst this study points to a novel, unexplained, yet controversial adaptation to cold it is important to remember the major differences in physiology, and cellular processes in animals housed at different ambient temperatures [14]. These differences will likely be exacerbated in animals who have been raised at thermoneutrality from weaning and it is not entirely unexpected that the physiological response to a commonly studied stimulus would be different in this scenario. It is clear that the early life environment, and early life stressors, impact adult physiology and susceptibility to disease, including obesity, and important adaptations during the developmental period may underlie the adaptations seen here. Despite aiming to mimic human physiology this work cannot of course recapitulate the human in-utero, and birth environment and there may be other key developmental changes in humans during this period that are not applicable here. Further, rearing temperature of rats is associated with changes to sympathoadrenal activity and rats are susceptible to obesity in both a strain, and sex-dependent manner [18, 38, 39]. It will be important in future to determine if this effect is not only species specific, but strain and sex specific as we look to untangle aspects of this biology to promote healthy expansion of adipose tissue in humans.

Conclusion

In summary, we show that chronic exposure to mild-cold following chronic suppression of BAT drives weight gain and the deposition of large quantities of subcutaneous AT. Whilst the precise mechanism is not clear, this work points towards a novel response whereby animals increase body weight and fat mass in response to a reduction in ambient temperature. We propose that chronic suppression of BAT from weaning, using thermoneutral housing and an obesogenic diet, changes the physiological response to cold in the obese state. Instead, humanised animals deposit adipose tissue and gain weight, an effect not seen with YM-178, suggesting a direct effect of temperature, where an insulative mechanism is potentially recruited when a thermogenic response is absent.

Methods

Animals, cold exposure and YM-178 treatment

All studies were approved by the University of Nottingham Animal Welfare and Ethical Review Board and were carried out in accordance with the UK Animals (Scientific Procedures) Act of 1986 (PPL no.). Eighteen male Sprague-Dawley rats aged 3 weeks were obtained from Charles River (Kent, UK) and housed immediately at thermoneutrality (c.28°C), on a high-fat diet (HFD; 45%, 824018 SDS, Kent, UK), under a 12:12-hour reverse light-dark cycle (lights off at 08:00). These conditions were chosen so as to closer mimic human physiology [3], minimise animal stress and maximise data quality and translatability [40]. At 12 weeks of age, all animals were randomised to 4 weeks of standard housing temperature (20°C, n=6), YM-178 (28°C+β3, at a clinically relevant dose of 0.75mg/kg/day, n=6) administration or HFD controls (28°C, n=6). In adherence to the National Centre for the Replacement, Refinement and Reduction of Animals in Research (NC3Rs), this experiment was ran alongside our work looking at the effect of exercise training on 'browning' and utilised the same cohort of control HFD animals [41].

Metabolic assessment and tissue collection

All animals were placed in an open-circuit calorimeter (CLAMS: Columbus Instruments, Linton Instrumentation, UK) for the final 48h to enable the assessment of whole body metabolism [42]. All animals were then weighed and fasted overnight prior to euthanasia by rising CO_2 gradient. BAT, perivascular BAT (PVAT) from the thoracic aorta and IWAT were then rapidly dissected, weighed, snap-frozen in liquid nitrogen and stored at -80°C for subsequent analysis.

Histology

Adipose tissue histology was performed as previously described [7]. Briefly, BAT and IWAT were fixed in formalin, embedded in wax using an Excelsior ES processor (Thermo-Fisher) and stained using haematoxylin and eosin (Sigma-Aldrich). Between 3 and 5 random sections were then imaged at 10x with an Olympus BX40 microscope and adipocyte size was quantified using Adiposoft [43].

Gene expression analysis

Total RNA was extracted from each fat depot using the RNeasy Plus Micro extraction kit (Qiagen, West Sussex, UK) using an adapted version of the single step acidified phenol-chloroform method. RT-qPCR was carried out as previously described using rat-specific oligonucleotide primers (Sigma) or FAM-MGB Taqman probes [42]. Gene expression was

341 determined using the GeNorm algorithm against two selected reference genes;
342 *RPL19:RPL13a in BAT* and IWAT (stability value M = 0.163 in BAT and 0.383 in IWAT) and
343 RPL19:HPRT1 in PVAT (stability value M = 0.285).

344 ***Serum analysis***

345 Glucose (GAGO-20, Sigma Aldrich, Gillingham, UK), triglycerides (LabAssay Trigylceride,
346 Wako, Neuss, Germany), non-esterified fatty acids (NEFA-HR(2), Wako, Neuss, Germany),
347 insulin (80-INSRT-E01, Alpco, Salem, NH, USA) and leptin (EZRL-83K, Merck, Darmstadt,
348 Germany) were measured as previously described following manufacturer's instructions [7].

349 ***Adipose tissue proteomics***

350 Protein extraction, clean up and trypsinisation was performed on 50-100 mg of frozen tissue
351 (n=4/group) was homogenised in 500 µL CellLytic MT cell lysis buffer (Sigma, C3228) prior
352 to removal of lipid and other contaminants using the ReadyPrep 2D cleanup Kit (Biorad,
353 1632130) [42]. Samples were then subjected to reduction, alkylation and overnight
354 trypsinisation following which they were dried down at 60°C for 4 h and stored at 80°C
355 before resuspension in LCMS grade 5% acetonitrile in 0.1% formic acid for subsequent
356 analysis. Analysis by mass spectrometry was carried out on a SCIEX TripleTOF 6600
357 instrument [44] with samples analysed in both SWATH (Data Independent Acquisition) and
358 IDA (Information Dependent Acquisition) modes for quantitation and spectral library
359 generation respectively. IDA data was searched together using ProteinPilot 5.0.2 to
360 generate a spectral library and SWATH data was analysed using Sciex OneOmics software
361 [45] extracted against the locally generated library as described previously [42].

362 ***Statistical analysis***

363 Statistical analysis was performed in GraphPad Prism version 8.0 (GraphPad Software, San
364 Diego, CA). Data are expressed as Mean±SEM with details of specific statistical tests in
365 figure legends. Despite prior use of the control group to understand the impact of exercise
366 training only the groups included in this paper were utilised for analyses [7]. Functional
367 analysis of the proteome was performed using the Advaita Bioinformatic iPathwayGuide
368 software (www.advaitabio.com/ipathwayguide.html) (fold change ± 0.5 and confidence score
369 cut-off of 0.75). Significantly impacted biological processes and molecular functions were
370 analysed in the context of the Gene Ontology Consortium database (2017-Nov) [46]. The
371 Elim pruning method, which removes genes mapped to a significant GO term from more
372 general (higher level) GO terms, was used to overcome the limitation of errors introduced by
373 considering genes multiple times [47]. Pathway analysis was carried out using the
374 ReactomePA package on R Studio (version 3.6.2) with a false discovery rate of <0.1.

Availability of data and material: The datasets used and analysed during the current study are available from the corresponding author on reasonable request.

Authors' contributions: P.A., H.B. and M.E.S. conceived the study and attained the funding; P.A. and M.E.S. developed and designed the experiments; P.A, J.E.L, I.L, A.K.M, I.B, R.C and D. J. B. performed the experiments; P.A., A.K.M. and D.J.B. analyzed the data; P.A. and M.E.S. wrote the paper which was revised critically by D.J.B., H.B., F.J.P.E, and J.E.L. for important intellectual content. All authors read and approved the final manuscript.

Funding: The British Heart Foundation [grant number FS/15/4/31184/].

References

1. Chechi, K., W. van Marken Lichtenbelt, and D. Richard, *Brown and beige adipose tissues: phenotype and metabolic potential in mice and men.* J Appl Physiol (1985), 2018. **124**(2): p. 482-496.
2. Gordon, C.J., *The mouse thermoregulatory system: Its impact on translating biomedical data to humans.* Physiol Behav, 2017. **179**: p. 55-66.
3. Kalinovich, A.V., et al., *UCP1 in adipose tissues: two steps to full browning.* Biochimie, 2017. **134**: p. 127-137.
4. de Jong, J.M.A., et al., *Human brown adipose tissue is phenocopied by classical brown adipose tissue in physiologically humanized mice.* Nature Metabolism, 2019. **1**(8): p. 830-843.
5. Symonds, M.E., M. Pope, and H. Budge, *The Ontogeny of Brown Adipose Tissue.* Annu Rev Nutr, 2015. **35**: p. 295-320.
6. Iannaccone, P.M. and H.J. Jacob, *Rats!* Dis Model Mech, 2009. **2**(5-6): p. 206-10.
7. Aldiss, P., et al., *Exercise Training in Obese Rats Does Not Induce Browning at Thermoneutrality and Induces a Muscle-Like Signature in Brown Adipose Tissue.* Frontiers in Endocrinology, 2020. **11**(97).
8. Tsiloulis, T., et al., *No evidence of white adipocyte browning after endurance exercise training in obese men.* Int J Obes (Lond), 2018. **42**(4): p. 721-727.
9. O'Mara, A.E., et al., *Chronic mirabegron treatment increases human brown fat, HDL cholesterol, and insulin sensitivity.* J Clin Invest, 2020.
10. Finlin, B.S., et al., *The beta3-adrenergic receptor agonist mirabegron improves glucose homeostasis in obese humans.* J Clin Invest, 2020.
11. Raun, S.H., et al., *Housing temperature influences exercise training adaptations in mice.* bioRxiv, 2019: p. 651588.
12. McKie, G.L., et al., *Housing temperature affects the acute and chronic metabolic adaptations to exercise in mice.* J Physiol, 2019.
13. Clayton, Z.S. and C.E. McCurdy, *Short-term thermoneutral housing alters glucose metabolism and markers of adipose tissue browning in response to a high-fat diet in lean mice.* Am J Physiol Regul Integr Comp Physiol, 2018. **315**(4): p. R627-R637.
14. Hylander, B.L. and E.A. Repasky, *Thermoneutrality, Mice, and Cancer: A Heated Opinion.* Trends Cancer, 2016. **2**(4): p. 166-175.
15. Rowland, L.A., et al., *Sarcolipin and uncoupling protein 1 play distinct roles in diet-induced thermogenesis and do not compensate for one another.* Obesity (Silver Spring), 2016. **24**(7): p. 1430-3.
16. Stern, J.S., et al., *Scapular brown fat removal enhances development of adiposity in cold-exposed obese Zucker rats.* Am J Physiol, 1984. **247**(5 Pt 2): p. R918-26.
17. Yoo, H.S., et al., *Intermittent cold exposure enhances fat accumulation in mice.* PLoS One, 2014. **9**(5): p. e96432.
18. Young, J.B. and Y. Shimano, *Effects of rearing temperature on body weight and abdominal fat in male and female rats.* Am J Physiol, 1998. **274**(2): p. R398-405.
19. Nilaweera, K.N. and J.R. Speakman, *Regulation of intestinal growth in response to variations in energy supply and demand.* Obes Rev, 2018. **19 Suppl 1**: p. 61-72.
20. Price, E.R., et al., *Cold exposure increases intestinal paracellular permeability to nutrients in the mouse.* J Exp Biol, 2013. **216**(Pt 21): p. 4065-70.
21. Chevalier, C., et al., *Gut Microbiota Orchestrates Energy Homeostasis during Cold.* Cell, 2015. **163**(6): p. 1360-74.
22. Fischer, A.W., et al., *No insulating effect of obesity.* Am J Physiol Endocrinol Metab, 2016: p. ajpendo 00093 2016.

23. Jay, O. and D. Raubenheimer, *Some problems with translating the insulating effect of obesity from mice to men.* Am J Physiol Endocrinol Metab, 2016. **311**(3): p. E638.
24. Fischer, A.W., et al., *Reply to letter to the editor: at thermoneutrality, neither the lean nor the obese freeze.* Am J Physiol Endocrinol Metab, 2016. **311**(3): p. E639.
25. Tang, Q.Q., T.C. Otto, and M.D. Lane, *Mitotic clonal expansion: a synchronous process required for adipogenesis.* Proc Natl Acad Sci U S A, 2003. **100**(1): p. 44-9.
26. Merkestein, M., et al., *FTO influences adipogenesis by regulating mitotic clonal expansion.* Nat Commun, 2015. **6**: p. 6792.
27. Hou, X., et al., *CDK6 inhibits white to beige fat transition by suppressing RUNX1.* Nat Commun, 2018. **9**(1): p. 1023.
28. Vishvanath, L. and R.K. Gupta, *Contribution of adipogenesis to healthy adipose tissue expansion in obesity.* J Clin Invest, 2019. **129**(10): p. 4022-4031.
29. Loh, R.K.C., et al., *Acute metabolic and cardiovascular effects of mirabegron in healthy individuals.* Diabetes Obes Metab, 2019. **21**(2): p. 276-284.
30. Baskin, A.S., et al., *Regulation of Human Adipose Tissue Activation, Gallbladder Size, and Bile Acid Metabolism by a beta3-Adrenergic Receptor Agonist.* Diabetes, 2018. **67**(10): p. 2113-2125.
31. Cypess, A.M., et al., *Activation of human brown adipose tissue by a beta3-adrenergic receptor agonist.* Cell Metab, 2015. **21**(1): p. 33-8.
32. Finlin, B.S., et al., *Human adipose beiging in response to cold and mirabegron.* JCI Insight, 2018. **3**(15).
33. Au-Yong, I.T., et al., *Brown adipose tissue and seasonal variation in humans.* Diabetes, 2009. **58**(11): p. 2583-7.
34. Gelinas, J.N., et al., *ERK and mTOR signaling couple beta-adrenergic receptors to translation initiation machinery to gate induction of protein synthesis-dependent long-term potentiation.* J Biol Chem, 2007. **282**(37): p. 27527-35.
35. Hostrup, M., et al., *Beta2 -adrenoceptor agonist salbutamol increases protein turnover rates and alters signalling in skeletal muscle after resistance exercise in young men.* J Physiol, 2018. **596**(17): p. 4121-4139.
36. Puzzo, D., et al., *CL316,243, a beta3-adrenergic receptor agonist, induces muscle hypertrophy and increased strength.* Sci Rep, 2016. **5**: p. 37504.
37. Emery, P.W., et al., *Chronic effects of beta 2-adrenergic agonists on body composition and protein synthesis in the rat.* Biosci Rep, 1984. **4**(1): p. 83-91.
38. Young, J.B., J. Weiss, and N. Boufath, *Effects of rearing temperature on sympathoadrenal activity in young adult rats.* Am J Physiol Regul Integr Comp Physiol, 2002. **283**(5): p. R1198-209.
39. White, C.L., et al., *Effect of a high or low ambient perinatal temperature on adult obesity in Osborne-Mendel and S5B/Pl rats.* Am J Physiol Regul Integr Comp Physiol, 2005. **288**(5): p. R1376-84.
40. Hawkins, P. and H.D.R. Golledge, *The 9 to 5 Rodent - Time for Change? Scientific and animal welfare implications of circadian and light effects on laboratory mice and rats.* J Neurosci Methods, 2018. **300**: p. 20-25.
41. Aldiss, P., et al., *Exercise does not induce browning of WAT at thermoneutrality and induces an oxidative, myogenic signature in BAT.* bioRxiv, 2019: p. 649061.
42. Aldiss, P., et al., *Interscapular and Perivascular Brown Adipose Tissue Respond Differently to a Short-Term High-Fat Diet.* 2019.
43. Galarraga, M., et al., *Adiposoft: automated software for the analysis of white adipose tissue cellularity in histological sections.* J Lipid Res, 2012. **53**(12): p. 2791-6.
44. Mele, L., et al., *A new inhibitor of glucose-6-phosphate dehydrogenase blocks pentose phosphate pathway and suppresses malignant proliferation and metastasis in vivo.* Cell Death Dis, 2018. **9**(5): p. 572.

45. Lambert, J.P., et al., *Mapping differential interactomes by affinity purification coupled with data-independent mass spectrometry acquisition.* Nat Methods, 2013. **10**(12): p. 1239-45.
46. Ashburner, M., et al., *Gene ontology: tool for the unification of biology. The Gene Ontology Consortium.* Nat Genet, 2000. **25**(1): p. 25-9.
47. Alexa, A., J. Rahnenfuhrer, and T. Lengauer, *Improved scoring of functional groups from gene expression data by decorrelating GO graph structure.* Bioinformatics, 2006. **22**(13): p. 1600-7.

Table 1. Full list of differentially regulated proteins in BAT

GeneID	Gene name	logfc	adjpv
20°C			
80754	Rabep2	3.69	6.35E-05
114122	Vcan	2.74	0.000269
292073	Galns	-2.75	0.00027
64012	Rad50	1.50	0.000288
171139	Timm9	-1.94	0.00037
295088	Gmps	0.67	0.000396
81716	Ggcx	1.44	0.000639
25622	Ptpn11	-2.47	0.000975
289590	Ociad1	-1.41	0.000988
29384	H2afy	-1.15	0.001077
28°C+B3			
116689	Ptpn6	-3.56	0.000154
25650	Atp1b1	-1.40	0.000303
59108	Mb	2.71	0.000548
306262	Btd	2.72	0.000735
501167	Gmppa	1.58	0.000934
64528	Golga2	0.98	0.001723
287633	Lrrc59	-0.62	0.002902
81726	Mvd	-3.82	0.004012
363425	Cav2	-2.41	0.004547
114559	Arhgef7	-1.54	0.005187

Table 2. Full list of GO terms enriched in BAT

goId	goName	countDE	countAll	pv_elim
20°C				
Biological Process				
GO:0000122	negative regulation of transcription from RNA polymerase II promoter	14	40	0.008
GO:0003006	developmental process involved in reproduction	20	68	0.0146
GO:0071786	endoplasmic reticulum tubular network organization	3	4	0.0209
GO:0019098	reproductive behavior	3	4	0.0209
GO:0006544	glycine metabolic process	3	4	0.0209
GO:0016226	iron-sulfur cluster assembly	3	4	0.0209
GO:0090068	positive regulation of cell cycle process	7	17	0.0231
GO:0046323	glucose import	6	14	0.0285
GO:0001932	regulation of protein phosphorylation	32	129	0.0316
GO:0098969	neurotransmitter receptor transport to postsynaptic membrane	2	2	0.0333
Molecular Function				
GO:0000980	RNA polymerase II distal enhancer sequence-specific DNA binding	4	5	0.0046
GO:0030984	kininogen binding	3	3	0.006
GO:0031492	nucleosomal DNA binding	4	6	0.0119
GO:0001846	opsonin binding	3	4	0.0207
GO:0005212	structural constituent of eye lens	3	4	0.0207
GO:0016634	oxidoreductase activity, acting on the CH-CH group of donors, oxygen as acceptor	3	4	0.0207
GO:0016831	carboxy-lyase activity	5	10	0.022
GO:0016746	transferase activity, transferring acyl groups	9	25	0.0259
GO:0004616	phosphogluconate dehydrogenase (decarboxylating) activity	2	2	0.0331
GO:0008484	sulfuric ester hydrolase activity	2	2	0.0331
Cellular Component				
GO:0042582	azurophil granule	4	4	0.0011
GO:0000790	nuclear chromatin	12	27	0.0014
GO:0031616	spindle pole centrosome	3	4	0.0209
GO:0000786	nucleosome	5	10	0.0223
GO:0042719	mitochondrial intermembrane space protein transporter complex	2	2	0.0333
GO:0001740	Barr body	2	2	0.0333
GO:0072687	meiotic spindle	2	2	0.0333
GO:0034751	aryl hydrocarbon receptor complex	2	2	0.0333
GO:0043196	varicosity	2	2	0.0333
GO:0001931	uropod	3	5	0.0453

28°C+B3				
Biological Process				
GO:0003009	skeletal muscle contraction	5	7	0.0015
GO:0051897	positive regulation of protein kinase B signaling	6	11	0.0034
GO:0010677	negative regulation of cellular carbohydrate metabolic process	3	3	0.0039
GO:1901896	positive regulation of calcium-transporting ATPase activity	3	3	0.0039
GO:0032781	positive regulation of ATPase activity	9	15	0.0055
GO:0050873	brown fat cell differentiation	3	4	0.0138
GO:0006937	regulation of muscle contraction	8	22	0.0147
GO:0071560	cellular response to transforming growth factor beta stimulus	8	22	0.0147
GO:0060048	cardiac muscle contraction	6	15	0.0209
GO:0048193	Golgi vesicle transport	12	42	0.024
Molecular Function				
GO:0035259	glucocorticoid receptor binding	3	4	0.013
GO:0001671	ATPase activator activity	3	4	0.013
GO:0008134	transcription factor binding	15	55	0.016
GO:0050431	transforming growth factor beta binding	2	2	0.024
GO:0031730	CCR5 chemokine receptor binding	2	2	0.024
GO:0031014	troponin T binding	2	2	0.024
GO:0005044	scavenger receptor activity	3	5	0.029
GO:0019905	syntaxin binding	4	9	0.037
GO:0016779	nucleotidyltransferase activity	4	9	0.037
GO:0004888	transmembrane signaling receptor activity	4	9	0.037
Cellular Component				
GO:0005887	integral component of plasma membrane	12	32	0.002
GO:0030134	COPII-coated ER to Golgi transport vesicle	5	9	0.0067
GO:0005861	troponin complex	2	2	0.0245
GO:0001741	XY body	2	2	0.0245
GO:0043596	nuclear replication fork	3	5	0.0299
GO:0044295	axonal growth cone	3	5	0.0299
GO:0016459	myosin complex	5	13	0.0399

Table 3. Full list of differentially regulated proteins in WAT

GeneID	Gene name	logfc	adjpv
20°C			
117028	Bin1	-2.79	8.97E-06
304290	Kdelr2	-2.68	4.47E-05
24667	Ppm1b	-2.65	0.000108
84114	Agps	-1.35	0.000125
84401	Puf60	-2.94	0.000753
300983	Abhd14b	0.94	0.000791
29218	Rcn2	-2.40	0.000854
290028	Osgep	-0.94	0.002064
24230	Tspo	-2.34	0.00248
171452	Rab3il1	-2.15	0.00629
28°C+B3			
83730	Vamp8	-3.75	6.93E-05
29521	Scamp1	1.51	0.000111
25116	Hsd11b1	0.92	0.000382
117045	Eif4e	-0.69	0.000942
25342	Oxtr	1.79	0.001104
298566	C1qa	0.85	0.001124
445268	Ufc1	-0.65	0.001133
78947	Gcs1	0.61	0.00204
266734	Npas4	0.87	0.004234
246303	Serbp1	0.78	0.004516

Table 4. Full list of GO terms enriched in WAT

goId	goName	countDE	countAll	pv_elim
20°C				
Biological Process				
GO:0030330	DNA damage response, signal transduction by p53 class mediator	5	6	0.0022
GO:0048711	positive regulation of astrocyte differentiation	3	3	0.0023
GO:0071498	cellular response to fluid shear stress	3	3	0.0023
GO:0032780	negative regulation of ATPase activity	3	3	0.0023
GO:0051607	defense response to virus	5	9	0.003
GO:0001822	kidney development	11	35	0.0036
GO:0050731	positive regulation of peptidyl-tyrosine phosphorylation	7	17	0.0037
GO:0002244	hematopoietic progenitor cell differentiation	3	4	0.0081
GO:0045577	regulation of B cell differentiation	3	4	0.0081
GO:0042130	negative regulation of T cell proliferation	3	4	0.0081
Molecular Function				
GO:0051287	NAD binding	11	31	0.0013
GO:0008144	drug binding	9	29	0.0101
GO:0005001	transmembrane receptor protein tyrosine phosphatase activity	2	2	0.0178
GO:0005521	lamin binding	3	5	0.0191
GO:0042393	histone binding	5	13	0.021
GO:0033613	activating transcription factor binding	3	6	0.0345
GO:0003857	3-hydroxyacyl-CoA dehydrogenase activity	3	6	0.0345
GO:0045296	cadherin binding	22	113	0.0365
GO:0004028	3-chloroallyl aldehyde dehydrogenase activity	2	3	0.0486
GO:0071933	Arp2/3 complex binding	2	3	0.0486
Cellular Component				
GO:0005884	actin filament	9	24	0.0021
GO:0032993	protein-DNA complex	5	11	0.0088
GO:0002102	podosome	7	14	0.013
GO:0016607	nuclear speck	8	26	0.0146
GO:0031209	SCAR complex	2	2	0.0172
GO:0042611	MHC protein complex	2	2	0.0172
GO:0005687	U4 snRNP	2	2	0.0172
GO:0005856	cytoskeleton	49	238	0.0284
GO:0030054	cell junction	41	216	0.0291
GO:0005681	spliceosomal complex	9	22	0.0311

28°C+B3				
Biological Process				
GO:0006953	acute-phase response	7	12	0.0035
GO:0000381	regulation of alternative mRNA splicing, via spliceosome	7	12	0.0035
GO:0034113	heterotypic cell-cell adhesion	8	12	0.0061
GO:0070528	protein kinase C signaling	4	5	0.0063
GO:0015671	oxygen transport	4	5	0.0063
GO:1901741	positive regulation of myoblast fusion	3	3	0.0077
GO:0070934	CRD-mediated mRNA stabilization	3	3	0.0077
GO:0007566	embryo implantation	6	12	0.0179
GO:0040007	growth	29	103	0.0209
GO:0071345	cellular response to cytokine stimulus	25	86	0.0211
Molecular Function				
GO:0003735	structural constituent of ribosome	24	62	0.00037
GO:0005344	oxygen carrier activity	4	5	0.00657
GO:0003730	mRNA 3'-UTR binding	8	18	0.01548
GO:0003682	chromatin binding	10	25	0.01623
GO:0140097	catalytic activity, acting on DNA	5	9	0.01908
GO:0042162	telomeric DNA binding	3	4	0.02688
GO:0045294	alpha-catenin binding	3	4	0.02688
GO:0004527	exonuclease activity	3	4	0.02688
GO:0003723	RNA binding	73	281	0.02734
GO:0019825	oxygen binding	4	7	0.03278
Cellular Component				
GO:0022625	cytosolic large ribosomal subunit	15	30	0.00018
GO:0016323	basolateral plasma membrane	14	32	0.00164
GO:0005833	hemoglobin complex	3	3	0.00782
GO:0005903	brush border	10	23	0.00812
GO:0030864	cortical actin cytoskeleton	9	20	0.00918
GO:0016327	apicolateral plasma membrane	3	4	0.02666
GO:0044451	nucleoplasm part	18	58	0.0269
GO:0005637	nuclear inner membrane	5	10	0.03167
GO:0035770	ribonucleoprotein granule	11	32	0.03804
GO:0097225	sperm midpiece	2	2	0.03953

570 **Figure legends**

571 **Figure 1.** Cold exposure (20°C) but not YM-178 (28°C+β3) drove weight gain and deposition
572 of BAT and inguinal white adipose tissue (IWAT) with no effect on serum metabolites or
573 thermogenic markers. (A) Final body weight, (B) 4 week intervention weight gain, (C) total fat
574 mass, (D) BAT mass, (E) IWAT mass, (F) 24h ambulatory activity, (G) 24h energy
575 expenditure, (H) 24h energy intake, (I-N) serum hormones and metabolites. (O-Q) Markers
576 of brown and beige adipose tissue in BAT, PVAT and IWAT, (R-W) select metabolic genes
577 in BAT and PVAT. Data expressed as mean ± SEM, n=4-5 per group. For comparison, data
578 was analysed by either one (A-E, H-Q), two-way ANOVA (F, R-W) or ANCOVA (G and H)
579 with Sidak post-hoc tests. Significance denoted as * <0.05; ** <0.01 or *** <0.001.

580

581 **Figure 2.** Histological and proteomics analysis of BAT following cold-exposure (20°C) and
582 YM-178 treatment (28°C+β3). (A-B) Histological analysis of BAT and lipid droplet area. (C)
583 Venn diagram of differentially regulated proteins. Reactome pathway analysis detailing
584 enriched pathways and interrelated networks in cold exposed (20°C, D-E) and YM-178
585 treated animals (28°C+β3, F-G). Data expressed as mean ± SEM, n=4-5 per group.
586 Adipocyte/lipid droplet area quantified using Adiposoft (28°C, n=8949; 20°C, 15512 and
587 28°C+β3, 12446). For comparison, data was analysed by one-way ANOVA (B) or using the
588 ReactomePA package (D-G). Significance denoted as **** <0.0001.

589

590 **Figure 3.** Histological and proteomics analysis of WAT following cold-exposure (20°C) and
591 YM-178 treatment (28°C+β3). (A-B) Histological analysis of BAT and lipid droplet area. (C)
592 Venn diagram of differentially regulated proteins. Reactome pathway analysis detailing
593 enriched pathways and interrelated networks in cold exposed (20°C, D-E) and YM-178
594 treated animals (28°C+β3, F-G). Data expressed as mean ± SEM, n=4-5 per group.
595 Adipocyte/lipid droplet area quantified using Adiposoft (28°C, n=750; 20°C, 553 and
596 28°C+β3, 527). For comparison, data was analysed by one-way ANOVA (B) or using the
597 ReactomePA package (D-G). Significance denoted as ** <0.01.

598

599 **Supplementary Figure 1.** Weight gain trajectory, adipose tissue depot and organ weights.
600 (A) Body weight gain trajectory from weaning and (B) gonadal, (C) mesenteric, (D)
601 retroperitoneal, (E) paracardial adipose tissues. (F) liver, (G) heart and (H) kidney mass. (I-J)
602 absolute energy expenditure and energy intake.

FIGURE 1

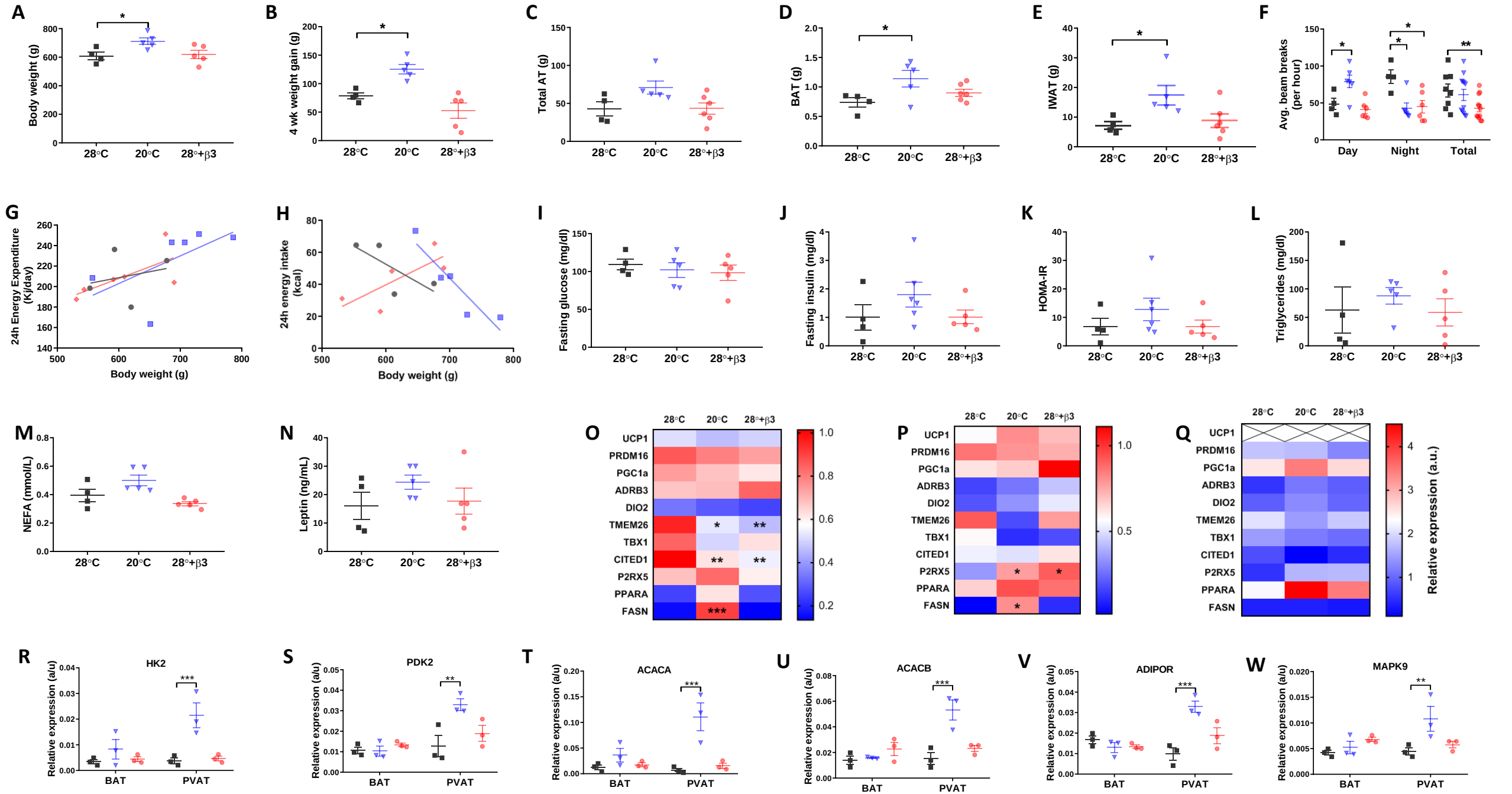
A
Body weight (g)
28°C
20°C
28°+β3
B
4 wk weight gain (g)
C
Total AT (g)
D
BAT (g)
E
IWAT (g)
F
Avg. beam breaks (per hour)
Day
Night
Total
G
24h Energy Expenditure (Kj/day)
Body weight (g)
H
24h energy intake (kcal)
I
Fasting glucose (mg/dl)
J
Fasting insulin (mg/dl)
K
HOMA-IR
L
Triglycerides (mg/dl)
M
NEFA (mmol/L)
N
Leptin (ng/mL)
O
P
Q
UCP1
PRDM16
PGC1a
ADRB3
DIO2
TMEM26
TBX1
CITED1
P2RX5
PPARA
FASN
Relative expression (a.u.)
R
HK2
S
PDK2
T
ACACA
U
ACACB
V
ADIPOR
W
MAPK9
Relative expression (a/u)
BAT
PVAT

FIGURE 2

A

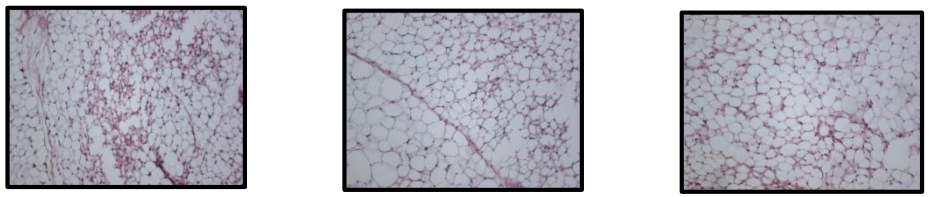

B

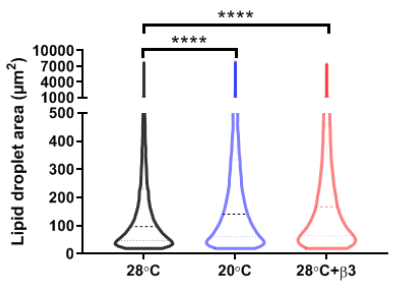

C

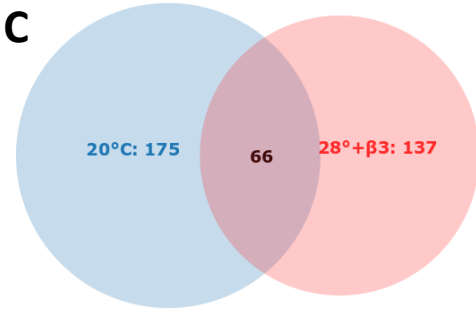

Reactome pathway and network analysis in BAT following cold-exposure

D

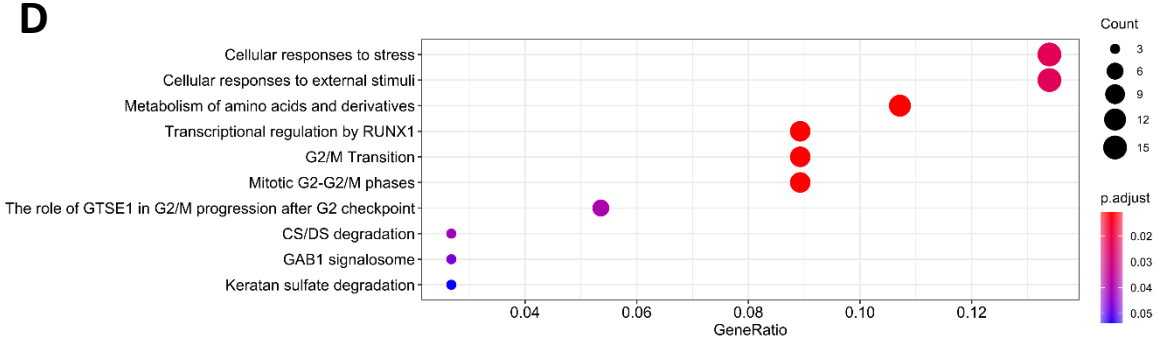

E

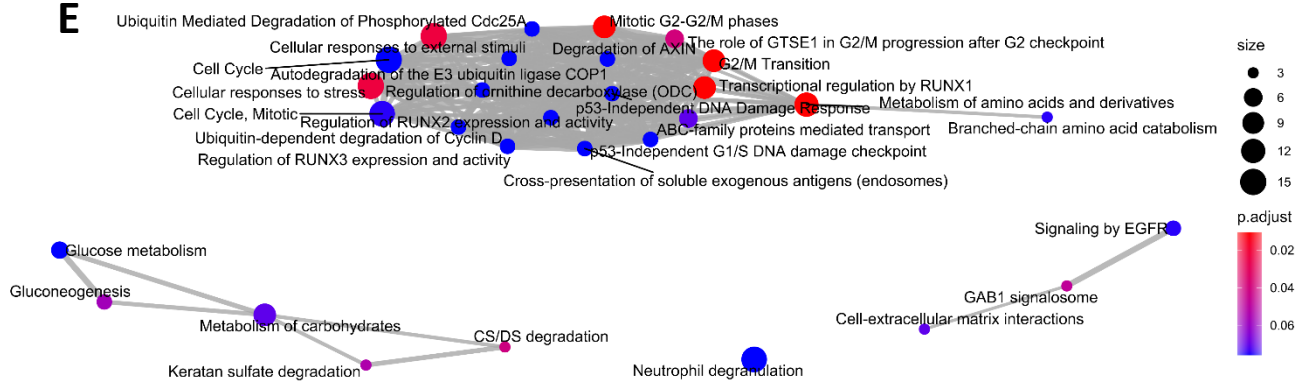

Reactome pathway and network analysis in BAT following Mirabegron

F

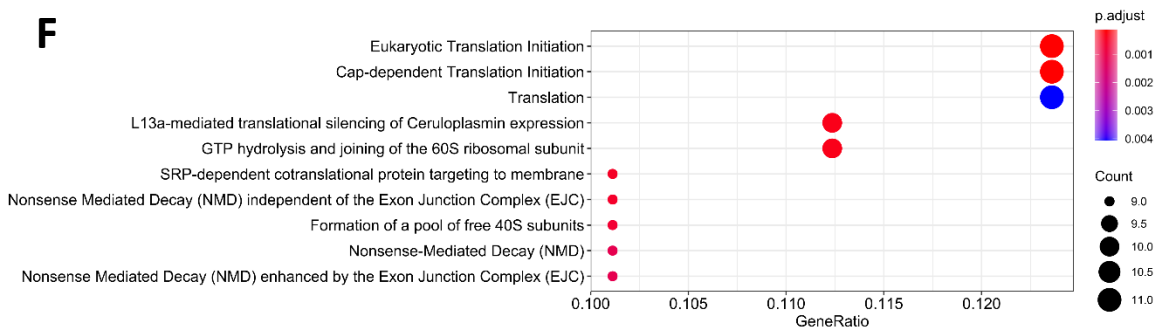

G

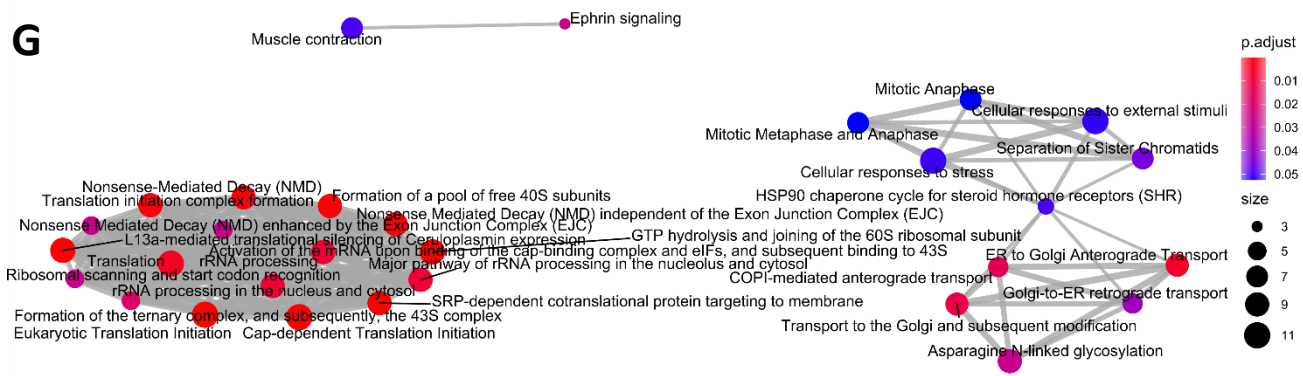

FIGURE 3

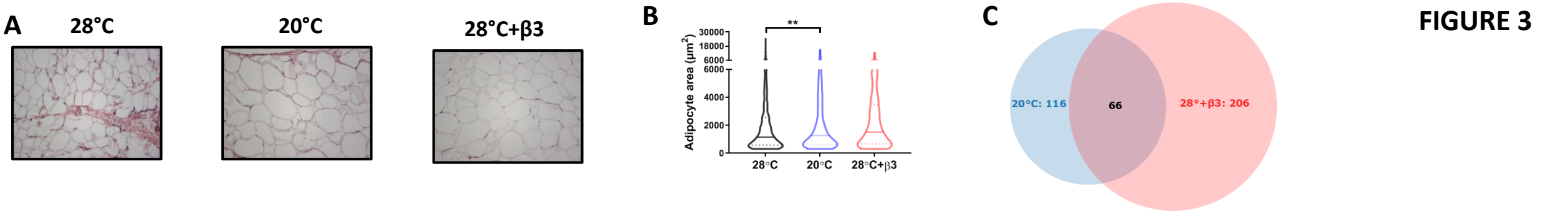

Reactome pathway and network analysis in WAT following cold-exposure

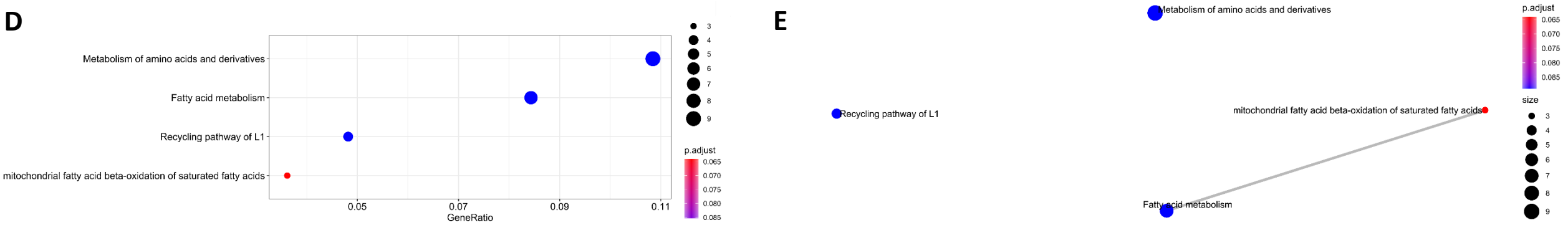

Reactome pathway and network analysis in WAT following Mirabegron

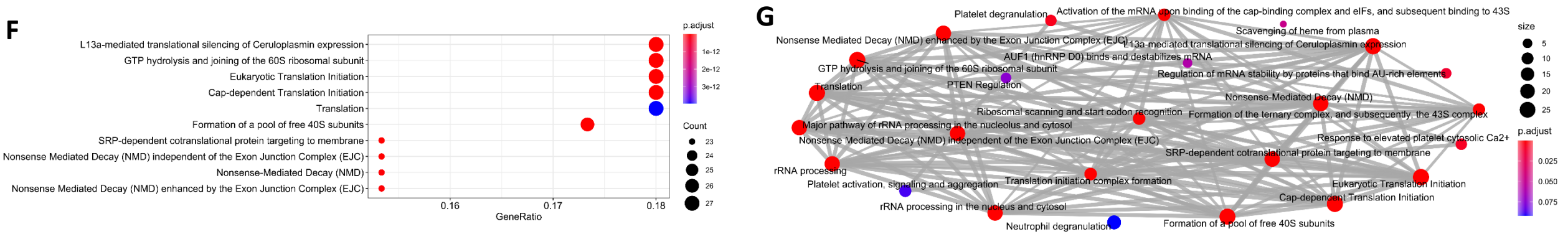

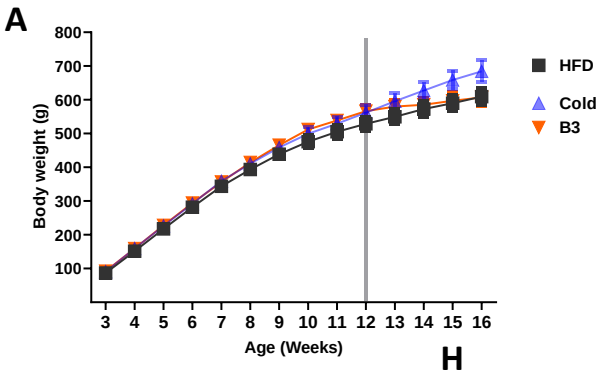
A
Body weight (g)
Age (Weeks)
HFD
Cold
B3

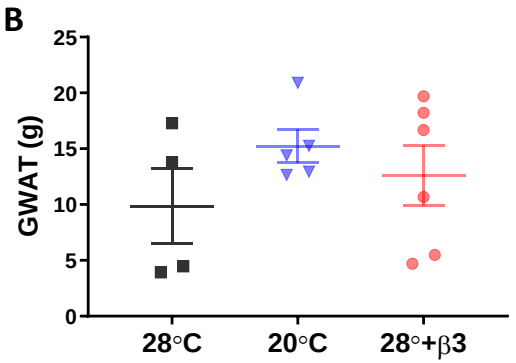
B
GWAT (g)
28°C
20°C
28°+β3

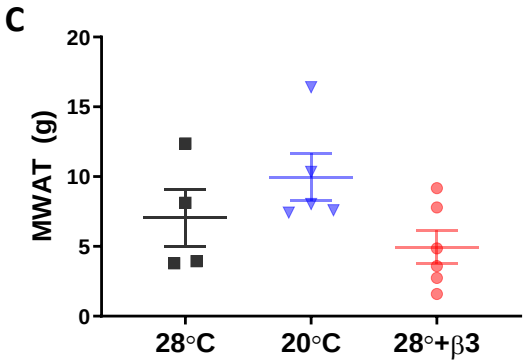
C
MWAT (g)
28°C
20°C
28°+β3

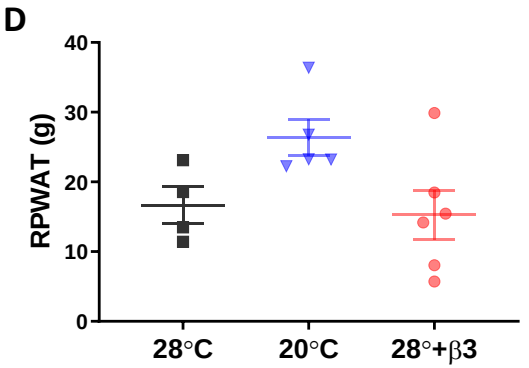
D
RPWAT (g)
28°C
20°C
28°+β3

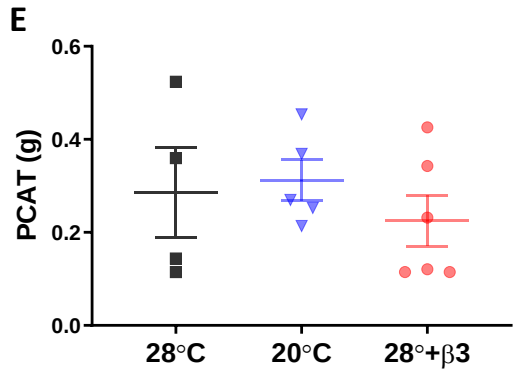
E
PCAT (g)
28°C
20°C
28°+β3

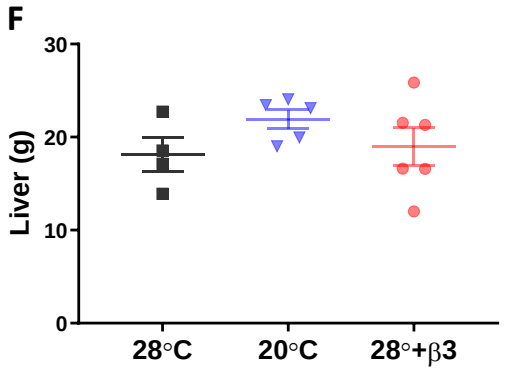
F
Liver (g)
28°C
20°C
28°+β3

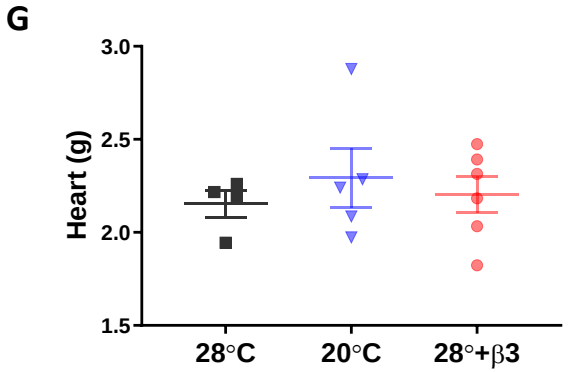
G
Heart (g)
28°C
20°C
28°+β3

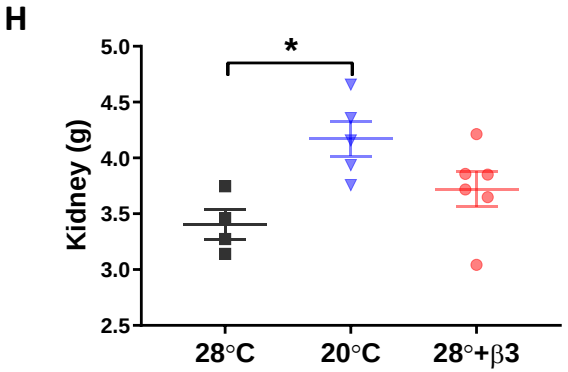
H
*
Kidney (g)
28°C
20°C
28°+β3

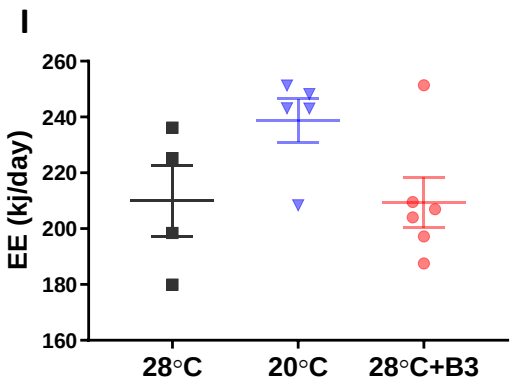
I
EE (kj/day)
28°C
20°C
28°C+B3

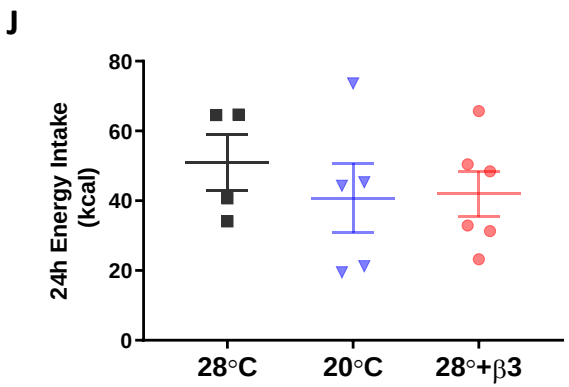
J
24h Energy Intake (kcal)
28°C
20°C
28°+β3